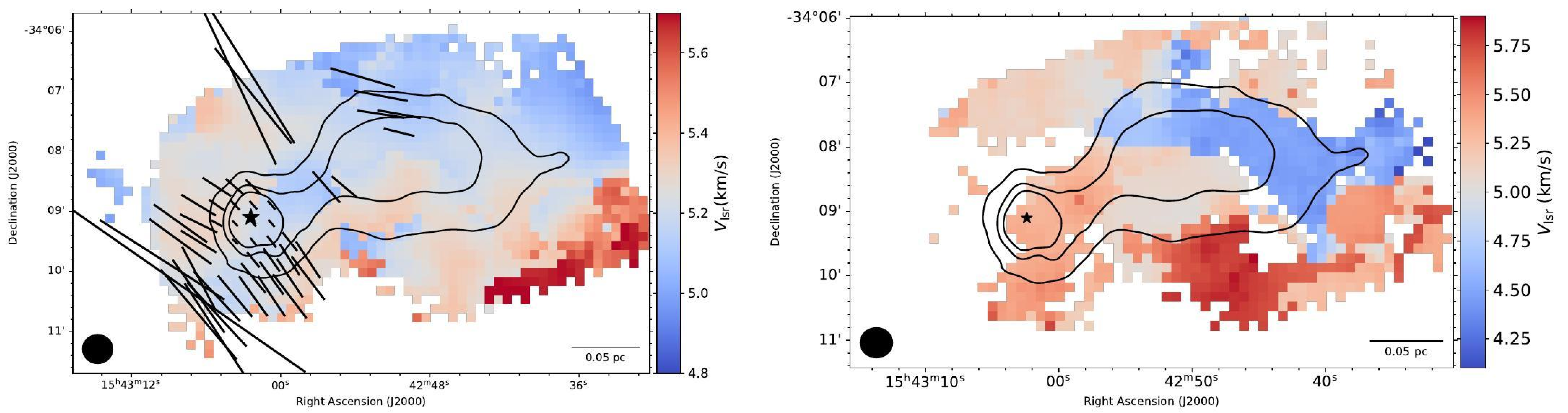

Fig. 6: Maps of kinematic parameters. Left panel: Bright component of centroid velocity map of $C^{18}O$ (2-1). Right panel: Centroid velocity map only showing the weak component of the Gaussian fitting. The black vectors represent the polarization angles, tilted by 90 degrees. The star shows the position of the protostar. The contours represent N(H_2) column density levels, as derived from Herschel data: [1.0,1.5,2.0] 10^{22} cm^{-2}.

We use this method and obtain the velocity gradient and the position angle with their uncertainties. The number of pixels used to carry out the fit is 9, which is appropriate for single-dish data that is Nyquist sampled (Caselli et al. 2002).

We only consider values with S/N > 3 in the final result for each velocity gradient value; the mean signal-to-noise ratio around the protostar position is 7. The mean velocity gradient magnitude distribution around the core peaks at 5.1 ± 0.7 km s^{-1} pc^{-1} and has a mean position angle of $(106 \pm 7)^\circ$ (counterclockwise from the north toward the east), which is shown as a yellow arrow in Fig. 4. We can see that this mean velocity gradient is consistent at the $3\times\sigma$ level to be perpendicular to the direction of the bipolar outflow found by Bjerkeli et al. (2016) (PA=35°). We assume that the total gradient is the rotational direction of the core. This method is implemented in a Python code which is available via open access on GitHub.[5]

4.4. $C^{18}O$ (2-1) line

Figure 6 represents the centroid velocity map obtained fitting the observed $C^{18}O$ (2-1) spectra. The left panel of Fig. 6 represents the brightest components of the Gaussian fitting, and as we discussed in Sect. 4.2, in some locations of the cloud $C^{18}O$ (2-1) gas reveals two velocity components. The right panel of Fig. 6 shows the second component, the one with lower intensity. Depending on the location on the map, this less bright component has red or blue velocities compared to the main component. The right panel of Fig. 6 shows that by moving from north to south the faint component is going to the red side of the brightest components. The red velocities appear mostly on the south of the filament and the west side of the protostar position. This is similar to our discussion in Sect. 4.2, where there are three components along the line of sight: the bright one associated with the core and two fainter ones, one in the north and one in the south of the filament.

A small velocity gradient can also be seen in the brightest component of the $C^{18}O$ (2-1) emission around the protostar in the east–west direction, in agreement with what we discuss in Sect. 4.3 for the DCO^+ (3-2) line, which is likely associated with the rotation of the core. For positions where N(H_2) > 2×10^{22} cm^{-2}, the mean value of the centroid velocity is $\langle V_{lsr} \rangle = 5.22$ km s^{-1} with an uncertainty 0.04 km s^{-1}. The V_{lsr} value at the west side of the core is 5.169 ± 0.005 km s^{-1} and increases toward the east side of the core up to the value 5.290 ± 0.003 km s^{-1}. These two values are calculated at the edge of the core, where the N(H_2) is equal to 2×10^{22} cm^{-2} (the inner contour in Fig. 6).

Frau et al. (2015) proposed for the Pipe nebula that the sharp changes in the magnetic field is produced by shocks between two clouds and, in comparison to the non-shocked gas, the column density and magnetic field strength double. Redaelli et al. (2019a) observed a sharp change in the magnetic field toward dust extension in the northwest direction of this cloud with respect to the core magnetic field. We predict that this is produced by merging two distinct clouds, two components of the $C^{18}O$ (2-1) line. These polarization vectors, which show different directions concerning the vectors in the core position, could result from the cloud collision.

4.5. Comparison between the $C^{18}O$ (2-1) and DCO^+ (3-2) kinematic

The result of the fitting procedure is shown in Fig. 7, where we present an image depicting a 3D position-position-velocity (PPV) diagram highlighting the distributions of DCO^+ (3-2) and $C^{18}O$ (2-1) gas throughout the cloud. Each data point illustrates the location and centroid velocity of an independent Gaussian component. The color of each data point relates to each spectral component (discussed in Sect. 4.2). Orange refers to DCO^+ (3-2) emitting gas, and the others refer to $C^{18}O$ (2-1) emitting gas. The velocity structure of the $C^{18}O$ (2-1) emission is quite complex. Four velocity components are displayed in total. Overall, for $C^{18}O$ (2-1) we used only two-component fitting, but here we display it in different categories. The blue data correspond to the brightest components of the $C^{18}O$ (2-1) gas, and the red and cyan points instead are related to the secondary fainter component, when it is located at lower and higher velocities, respectively, with respect to the brightest one.

We observe a systematic difference between the centroid velocity of DCO^+ (3-2) and the main component of $C^{18}O$ (2-1), suggesting that they are not tracing exactly the same gas. We speculate that this is related to the fact that one is an ion and the other is a neutral species, and they behave differently concerning the magnetic fields, or it could be because of the difference between their gas densities. It is important to note that if ions and neutrals behave differently at the same density, this indicates a violation of the flux-freezing assumption. We discuss this point in more detail in Sect. 5.

[5] https://github.com/jpinedaf/velocity_tools